This article is published in Plant Physiology Online, Plant Physiology Preview Section, which publishes manuscripts accepted for publication after they have been edited and the authors have corrected proofs, but before the final, complete issue is published online. Early posting of articles reduces normal time to publication by several weeks.

Vascularization, High-Volume Solution Flow, and Localized Roles for Enzymes of Sucrose Metabolism during Tumorigenesis by *Agrobacterium tumefaciens*[1]

Rebecca Wächter, Markus Langhans, Roni Aloni, Simone Götz, Anke Weilmünster, Ariane Koops, Leopoldine Temguia, Igor Mistrik, Jan Pavlovkin, Uwe Rascher, Katja Schwalm, Karen E. Koch, and Cornelia I. Ullrich*

Institute of Botany, Darmstadt University of Technology, Schnittspahnstrasse 3, 64287 Darmstadt, Germany (R.W., M.L., S.G., A.W., A.K., L.T., K.S., C.I.U.); Department of Plant Sciences, Tel Aviv University, Tel Aviv 69978, Israel (R.A.); Slovak Academy of Sciences, Department of Plant Physiology, Dúbravská cesta 14, 84223 Bratislava, Slovakia (I.M., J.P.); Columbia University, Biosphere 2 Center, P.O. Box 689, Oracle, Arizona 85623 (U.R.); and Department of Horticulture Sciences, University of Florida, P.O. Box 110690, Gainesville, Florida 32611 (K.E.K.)

Vascular differentiation and epidermal disruption are associated with establishment of tumors induced by *Agrobacterium tumefaciens*. Here, we address the relationship of these processes to the redirection of nutrient-bearing water flow and carbohydrate delivery for tumor growth within the castor bean (*Ricinus communis*) host. Treatment with aminoethoxyvinylglycine showed that vascular differentiation and epidermal disruption were central to ethylene-dependent tumor establishment. CO_2 release paralleled tumor growth, but water flow increased dramatically during the first 3 weeks. However, tumor water loss contributed little to water flow to host shoots. Tumor water loss was followed by accumulation of the osmoprotectants, sucrose (Suc) and proline, in the tumor periphery, shifting hexose-to-Suc balance in favor of sugar signals for maturation and desiccation tolerance. Concurrent activities and sites of action for enzymes of Suc metabolism changed: Vacuolar invertase predominated during initial import of Suc into the symplastic continuum, corresponding to hexose concentrations in expanding tumors. Later, Suc synthase (SuSy) and cell wall invertase rose in the tumor periphery to modulate both Suc accumulation and descending turgor for import by metabolization. Sites of abscisic acid immunolocalization correlated with both central vacuolar invertase and peripheral cell wall invertase. Vascular roles were indicated by SuSy immunolocalization in xylem parenchyma for inorganic nutrient uptake and in phloem, where resolution allowed SuSy identification in sieve elements and companion cells, which has widespread implications for SuSy function in transport. Together, data indicate key roles for ethylene-dependent vascularization and cuticular disruption in the redirection of water flow and carbohydrate transport for successful tumor establishment.

The significance of this research lies in the identification of functional relationships effecting the redirection of nutrient-bearing water flow and carbohydrate delivery necessary for tumor establishment by *Agrobacterium tumefaciens*. Early, ethylene-dependent changes in both tumor vascular development and epidermal disruption are shown here linked to key shifts in water flow, sugar gradients, and highly localized roles for enzymes of Suc metabolism.

The experimental system used in this work provided three distinct advantages: First, the robust, rapidly growing host species castor bean (*Ricinus communis*) can support production of unusually large tumors when induced by *A. tumefaciens*. The size of these stem tumors was invaluable to the functional analyses reported here.

Second, these tumors develop through a series of well-defined events. Initial development is triggered by the expression of the T-DNA-located genes encoding auxin and cytokinin synthesis (*iaaM*, *iaaH*, and *ipt*; Weiler and Schröder, 1987; Zambryski et al., 1989). The rapid tumor proliferation is maintained by a substantial differentiation of vascular bundles with phloem and xylem, functionally connected to the host bundles and by a dense net of phloem anastomoses (Aloni et al., 1995; Ullrich and Aloni, 2000). Tumors are typically transformed by up to 100% (Rezmer et al., 1999) and overproduce auxin and cytokinin (Veselov et al., 2003). This is accompanied by additional production of ethylene (Aloni et al., 1998; Wächter et al., 1999), jasmonic acid, and abscisic acid (ABA), with severe consequences for growth of host shoot and roots (Mistrik et al., 2000; Veselov et al., 2003).

[1] This work was supported by the Deutsch Forschungsgemeinschaft/Sonderforschungsbereich (grant no. 199 to C.I.U.).

* Corresponding author; e-mail uleb@bio.tu-darmstadt.de; fax 49–6151–164630.

Article, publication date, and citation information can be found at www.plantphysiol.org/cgi/doi/10.1104/pp.103.028142.

Third, this system can be readily manipulated by specifically altering ethylene perception, as shown for ethylene-insensitive *Never ripe* mutant tomato (*Lycopersicon esculentum*) plants that do not develop tumors when infected with *A. tumefaciens* (Aloni et al., 1998).

Here, treatment of developing tumors with the ethylene synthesis inhibitor aminoethoxyvinyl-Gly (AVG) demonstrated that vascularization and epidermal disruption were part of a critical, ethylene-dependent phase of establishment for tumors induced by *A. tumefaciens*.

For this reason, focus of the present work was directed toward mechanisms by which vascular development and cuticular rupture could affect tumor establishment. Vascularization is essential for efficient assimilate import from the host plant into the tumor parenchyma cells via symplastic phloem unloading of Suc in the tumor (Malsy et al., 1992; Pradel et al., 1996, 1999). In addition, acquisition of inorganic ions is enhanced by the auxin- and ethylene-dependent proliferation of vessel numbers at the host/tumor interface. At the same time, disruption of the tumor epidermis and cuticle together with the increased number of narrower vessels appeared to accelerate water flow through the tumor at the expense of the host shoot, as described by the gall constriction hypothesis (Aloni et al., 1995; Schurr et al., 1996). Finally, specific xylem parenchyma cells form at sites of considerable auxin and cytokinin concentrations (Veselov et al., 2003). Their high electrical membrane potential difference appears to be associated with efficient nutrient absorption out of the vessels into the tumor symplast (Pavlovkin et al., 2002).

One aim of the present study was to define the relationship between epidermal disruption and nutrient-bearing water flow, particularly in the context of competition for this resource between tumor and host leaves. Toward this end, a method was developed that allowed accurate quantification of the irregular tumor surface and its transpiration rate, and this was done during several weeks of tumor development. Direct evidence was thus obtained for a quantitative comparison of water flow through tumors and leaves and thus the significance of its balance for transpiration for tumor development and growth of the host plant shoot.

A second aim was to determine what changes occurred in effectors of Suc import and osmotic adjustment during vascular development in this distinctive sink for sugars and nutrient-bearing water flow. Enzymes of Suc metabolism and associated shifts in sugar gradients were quantified during development and at specific sites in the tumor to appraise their import and/or osmotic contributions. The Suc-cleaving enzymes, acid cell wall invertase (CWIN), acid vacuolar invertase (VIN), and Suc synthase (SuSy) can play crucial roles in carbohydrate partitioning to sink organs and in this capacity can provide substrates for osmotic adjustment or protection as well as energy expenditure for storage and growth (Koch, 1996; Xu et al., 1996; Tymowska-Lalanne and Kreis, 1998; van Bel, 2003). Genes for these enzymes also respond to plant growth regulators such as auxin and cytokinins (Weil and Rausch, 1990; Koch, 1996; Roitsch and Ehness, 2000). However, their role remained elusive (Koch, 1996). Therefore, we were interested to know the degree to which activity and localization of these enzymes corresponded to sugar concentration gradients and sites of previously defined phytohormone accumulation (Veselov et al., 2003), including here immunolocalization of ABA concentration gradients.

Analysis of this distinctive model system for high-volume solute and Suc transfer has provided several new insights into mechanisms underlying phloem functioning and import into these and other sink organs. First, successful establishment of these tumor sinks involves ethylene-induced transition to high-volume flow of solutes with essential inorganic nutrients, yet this itself does not appear responsible for host dwarfing. Second, sugar balance in actively growing tumors shifts in ratio from hexose to Suc, which would initially favor signals for cell division and expansion and later, those for maturation, storage, and desiccation tolerance. Third, VINs in these tumors appear to mediate this transition in sugar balance as well as symplastic import of Suc. CWINs contributed late in development at the tumor periphery, possibly aiding maintenance of turgor gradients favoring transport to the tumor surface. Finally, data here significantly extend our understanding of respiratory roles for SuSy, which included not only the high-Suc regions at the tumor periphery, but also xylem parenchyma cells ideally positioned for inorganic nutrient uptake, and both companion cells and sieve elements of phloem.

RESULTS

Vascularization and Cuticular Rupture

Vascular development and cuticular rupture appear to be two key steps in establishing solute flow into plant tumors such as those induced by *A. tumefaciens* (Aloni et al., 1995; Ullrich and Aloni, 2000). We therefore examined these two processes in a castor bean host (Fig. 1) that facilitates their in-depth analyses and comparison with other aspects of sink development. Successfully established tumors showed a markedly elaborated and strongly increased surface area (Fig. 1A, inset), associated with stunting of the host above the tumor (Fig. 1A). Shoot stunting is suggested to result from both direct and indirect effects of the gall on host transpiration, together with competition for solution flow by the tumor itself (Aloni et al., 1995; Schurr et al., 1996; Pavlovkin et al., 2002). Figure 1, B and C, shows that the epidermis

becomes severely disrupted in actively growing galls and that parenchyma is left with little or no structural barrier to water loss. Young tumors, however, can have largely intact epidermis and cuticle (stained red in Fig. 1B). To further explore timing and consequences of this change, a series of such micrographs (not shown) were rigorously analyzed to track epidermal integrity and to quantify increases in surface area (discussed below).

Figure 1D shows that tumor development was severely impaired by a 3-week external application of the ethylene biosynthesis inhibitor, AVG, to the infection site. This provides additional evidence supporting the critical role of ethylene in establishment of these sinks and extends earlier work of Aloni et al. (1998) and Wächter et al. (1999) by demonstrating that ethylene from the young tumor itself is the source of these responses. The epinastic bending of cotyledons on infected plants was also prevented by AVG application to the tumor site (Fig. 1D). In addition, microscopic analysis showed that vascularization was completely suppressed throughout the tumor in the presence of AVG. Only poorly growing and undifferentiated callus tissue developed (Fig. 1E).

Water and CO_2 Loss

The water vapor conductance (g_{H2O}) of tumors rose rapidly within the 1st week after infection (p.i.) with the strongest increase between the 2nd and 3rd week p.i. (Fig. 2A). The g_{H2O} increased to 54 mmol m^{-2} s^{-1} in 6-week-old tumors, whereas uninfected stems had a constant g_{H2O} between 2 and 8 mmol m^{-2} s^{-1}, independent of their age. Concurrent growth of tumors was sigmoidal (Fig. 2B), with some fresh weights rising above 80 g and some tumors reaching the size of tennis balls (approximately 8 cm in diameter). Changes in the highly irregular tumor surface area were quantified by thorough microscopic analysis (as in Fig. 1B) and were found to increase almost linearly with tumor growth (Fig. 2C). The g_{H2O} thus appears related to the tumor surface area, combined with the timing of rupture and break-up of epidermis and cuticle during the first 3 weeks of gall growth.

Table I compares water-loss parameters of tumors with those of leaves. The g_{H2O} of leaves of uninfected plants was about 360 mmol m^{-2} s^{-1} during the light period, i.e. 10 times that of tumors. During the dark period, g_{H2O} of the leaves decreased to 12 mmol m^{-2} s^{-1} and that of the tumors only slightly to 28 mmol m^{-2} s^{-1} on average. The net transpiration rate (J_{H2O}) of tumors was about seven times lower in light but was twice that of similarly aged control leaves in the dark. When considered on a whole-organ basis, water flow through tumors could thus contribute to a significant amount of water loss, but much less than that of leaves on healthy or infected plants.

The net CO_2 emission rate (J'_{CO2}) of uninfected stems varied between 1 and 2 μmol μmol g^{-1} fresh weight h^{-1} (Fig. 3) and did not change with exposure of the leaves to light or dark (data not shown). During earlier tumor development, the J'_{CO2} increased considerably, beginning 2 weeks after initiation and increasing continuously until reaching about 18 μmol CO_2 μmol g^{-1} fresh weight h^{-1} at 6 weeks p.i. Simultaneously, the dry weight to fresh weight ratio increased from 10% to 15% (data not shown). The mean rate of respiratory loss during the first 8 weeks of tumor growth was thus about 10 mg CO_2 g^{-1} fresh weight d^{-1}, or about 25% to 30% of the estimated carbohydrate demand by these sinks.

ABA Pattern

ABA distribution, detected in 3-week-old tumors by immunofluorescence with monoclonal antibodies, showed an interesting pattern throughout the tumor. Distinct fluorescence was detected around the vascular bundles (Fig. 1, F and H) and in the very peripheral cell layers (Fig. 1H). At cellular resolution, the ABA-specific fluorescence was localized in parenchyma cells adjacent to vessels (Fig. 1I). In host stems close to developing tumors, the strongest ABA-specific fluorescence was found in phloem companion cells (Fig. 1J) and in xylem parenchyma cells (Fig. 1K). Figure 1L shows the autofluorescence of lignified vessels of the same section as in Figure 1K, however, under 488-nm light. Control cross sections of the host stem treated with 1% (w/v) BSA instead of the primary ABA antibody and with the secondary antibody-Alexa 568 conjugate showed distinct autofluorescence of the lignified vessels only (Fig. 1M).

Suc, Hexose, and Pro Distribution

Suc concentration was highest in the outmost 1 to 2 mm of 6-week-old tumors and clearly decreased toward the center (Fig. 4A). This gradient was minimally evident in 3-week-old tumors, but steepened with tumor age (Fig. 4A). In contrast, an inverse gradient of hexose concentration was found in young tumors, with maximal levels decreasing from the tumor center toward the periphery (Fig. 4B). The gradient decreased with tumor age. Such inverse sugar gradients also appear within primary roots of maize (*Zea mays*), with steeper gradients in water-stressed seedlings (Sharp et al., 1990). Hexose to Suc shifts are also evident in developing seeds, where as Wobus and Weber (1999) proposed, hexoses favor cell division and expansion and Suc stimulates maturation and desiccation tolerance.

Transpiration increased dramatically during disruption of the epidermis and cuticle of the tumors (Fig. 1, A and C; Table I), and consequent production of compatible solutes could aid protection of tumor parenchyma from desiccation. Three to 4 weeks after tumor induction, the concentrations of Suc and Pro began to rise in the periphery, where they reached

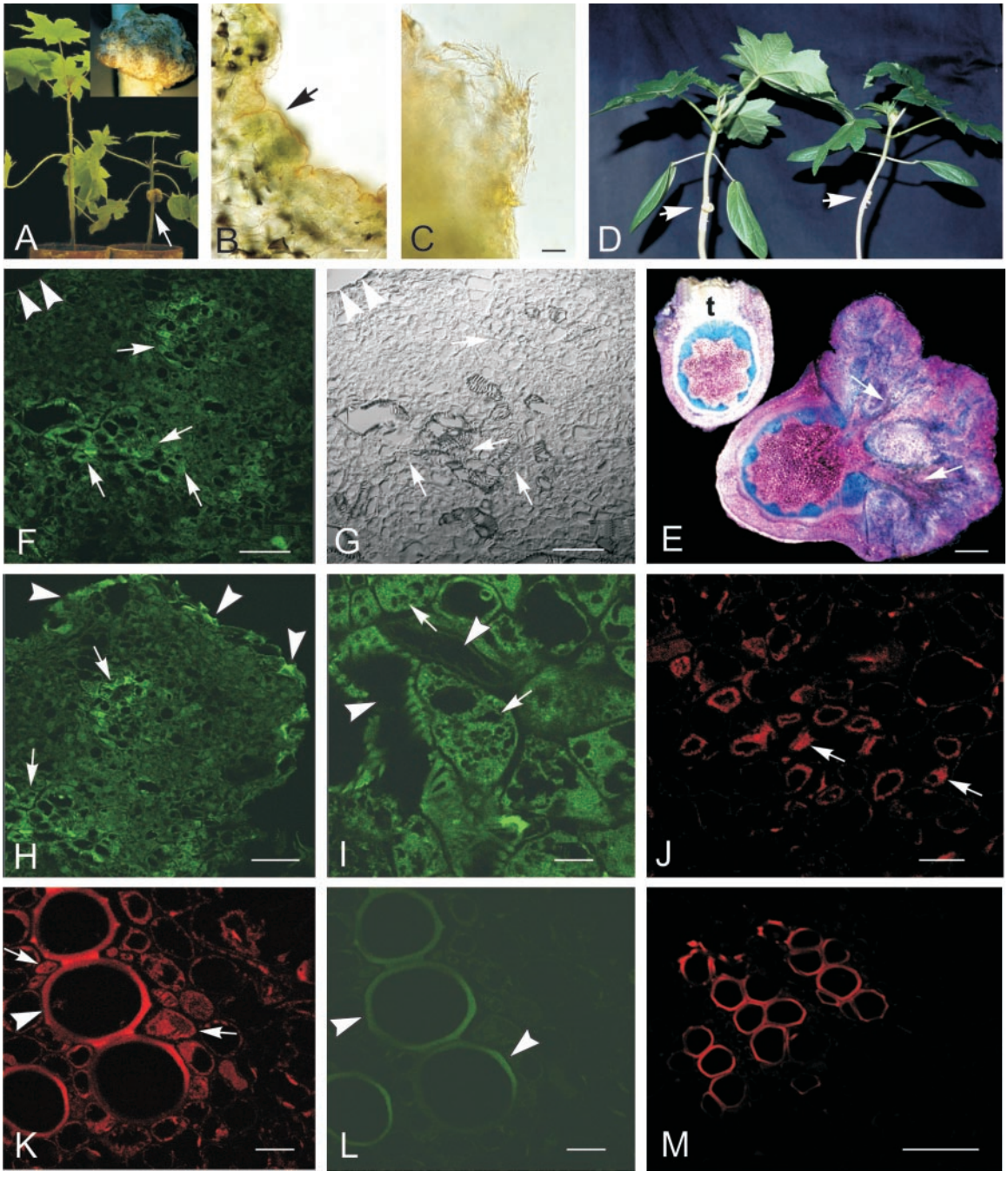

Figure 1. Morphological and structural changes of castor bean stem tumors and the impact of ethylene and ABA on their development. A, Growth retardation of castor bean plants (4-week-old) due to tumor development at the hypocotyl (arrow); inset, highly irregular surface of a 4-week-old tumor. B and C, Sections across the tumor margin, stained with Sudan III. B, Young tumor with intact cuticle (stained red, arrow). C, Older tumor with disrupted epidermis and without cuticle. D, Inhibition of tumor growth (arrow) by AVG treatment for 3 weeks without epinastic reaction of the cotyledons (right plant, +AVG); untreated infected plant with 3-week-old tumor (arrow) and epinastic reaction of the cotyledons (left plant, −AVG). E, Cross sections of 3-week-old tumors at the stem, treated with AVG (+AVG, left) and untreated (−AVG, right), stained with toluidine blue. Note the well-developed vascular bundles of the untreated tumor (arrows) and the undifferentiated poor callus of the AVG-treated tumor (t). F through M, ABA immunolocalization in 3-week-old tumor sections. F, By mouse hybridoma monoclonal antibodies and Alexa 488 (green) and Alexa 568 (red) fluorescent secondary antibody conjugates, ABA immunolocalization was strongest labeled around and within developing vascular bundles (arrows). Arrowheads mark the tumor periphery. G, Same section as F, viewed in differential interference contrast (DIC) mode. H, Besides the labeled tumor center (arrows), the very tumor periphery also showed strong ABA-specific fluorescence (arrowheads). I, Strongest ABA label was localized in xylem parenchyma cells (arrows), adjacent to tumor vessels (arrowheads). J through M, Cross

(*Legend continues on facing page.*)

respective levels of 20 and 40 times those in the control stem (Fig. 5, A and B). Both Suc and Pro concentrations in the tumor periphery were more than five times those in the tumor center (Fig. 5, A and B). The Pro concentration gradient from its maximum in the periphery toward the tumor center was steeper than that of Suc (Fig. 4, C versus A).

CWIN and VINs

As observed for net CO_2 emission, CWIN activity increased after a lag phase and was maximum at 6 to 7 weeks after tumor induction (Fig. 6A). Maximal activity was restricted to the peripheral cell layers at the outermost 1 to 2 mm of the tumor. The CWIN activity was 20 times less in the tumor center and 50 times less in the uninfected stem (Fig. 6A).

Maximum activity of the VIN was twice that of CWIN and peaked much earlier in tumor development (Fig. 6B). Early activity of VIN has also been observed in *Helianthus* sp. tumors (Kutschera et al., 2000). The activity in castor bean tumors was more than five times that of the control stem, independent of wounding, and gradually decreased during tumor growth. Activity was consistently higher in the tumor center than in its periphery in the later stages (Fig. 6B).

SuSy

SuSy activity increased within the 1st week after tumor induction (Fig. 7). In contrast, in rapidly necrotizing tumors of *Helianthus* sp., SuSy activity was very low and did not exceed that of the control stem (Kutschera et al., 2000). In castor bean tumors, SuSy was more than five times more active in tumors than in the control stem and higher in the periphery than in the tumor center (Fig. 7). Overall activity gradients within the tumor were less pronounced than those of the CWIN activity. Among the Suc-metabolizing enzymes investigated, VIN showed the greatest rates of Suc cleavage, with 17 nkat g^{-1} fresh weight, followed by CWIN with 8 nkat g^{-1} fresh weight and SuSy with 5 nkat g^{-1} fresh weight. The different activities of the Suc-cleaving enzymes in the tumor periphery and center were not due to differences in total protein content, because these were similar in both tissue types (Fig. 2D).

The resolution of immunolocalization of SuSy with polyclonal anti-*Sh1* and *Sus1*-protein antibodies in tissue sections of 2-week-old tumors showed a more distinct gradient and more precise localization in SuSy protein (Fig. 8) than could be achieved by activity measurements upon tissue dissection (Fig. 7). The highest fluorescence label was found in the tumor periphery, a tissue area that lacks vascular bundles in the castor bean system (Fig. 8, A and B). In the individual vascular bundles of the tumor, moderately fluorescent SuSy label was evident in the peripheral parenchyma and companion cells of the phloem immediately inside the encircling xylem (Fig. 8, C and D). At the tumor/host interface, the only xylem cells labeled were parenchyma cells in the tumor vascular bundles, no label was found in the multiseriate rays (Fig. 8, E, F, and top of G). In the control stem, SuSy label appeared in the cytoplasm of the companion cells and the thin cytoplasmic layer in the sieve elements.

The level of resolution possible in this system was exciting and extends earlier work of Nolte and Koch (1993) by showing that phloem SuSy includes labeling at or near the plasma membrane of the sieve elements (Fig. 8, G–I). SuSy label (green) was maximally evident in the cytoplasm of the companion cells, and also about 0.27 μm away, where the plasma membrane and/or adjacent cytoplasm of sieve elements was marked by red fluorescence conjugated to monoclonal antibodies specific for plasma membrane H^+-ATPase (Figs. 8, G–I, and 9). Quantification of red and green fluorescence confirmed the highly marginal localization of SuSy and plasma membrane H^+-ATPase in the sieve elements (Fig. 9).

DISCUSSION

The dual importance of work presented here lies in its identification of ethylene-dependent mechanisms for both water and Suc delivery to tumors induced by *A. tumefaciens*. For water, a pivotal disruption of epidermal integrity is shown here to coincide with dramatic increases in fluid flux and capacity for transfer of inorganic nutrients to the tumor. Direct contributions by this flow to concurrent stunting of the host shoot were calculated to be minimal. For Suc, critical changes in vascular development are shown to be linked to (a) a shift from hexose to Suc accumulation, (b) a transition from VIN to CWIN, and (c) previously unidentified sites of SuSy action in specific cells of both xylem and phloem.

Figure 1. (Legend continued from facing page) sections of the tumor adjacent host stem. J, Distinct ABA-indicating label was localized in the phloem, in companion cells (arrows). K, Distinct ABA label in xylem parenchyma cells (arrows) close to the autofluorescent vessels (arrowhead). L, Same section as in K, but viewed under 488-nm light, revealing strong autofluorescence of lignified vessels (arrowheads). M, Control cross section of a host stem vascular bundle, treated in the absence of the primary ABA antibody with 1% (w/v) bovine serum albumin (BSA) and the secondary Alexa 568 antibody conjugate, showing strong autofluorescence of lignified vessels. Upon request, DIC images for H through M will be made available. Bars in I through L = 20 μm; in B, C, F through H, and M = 80 μm; in E = 2 mm.

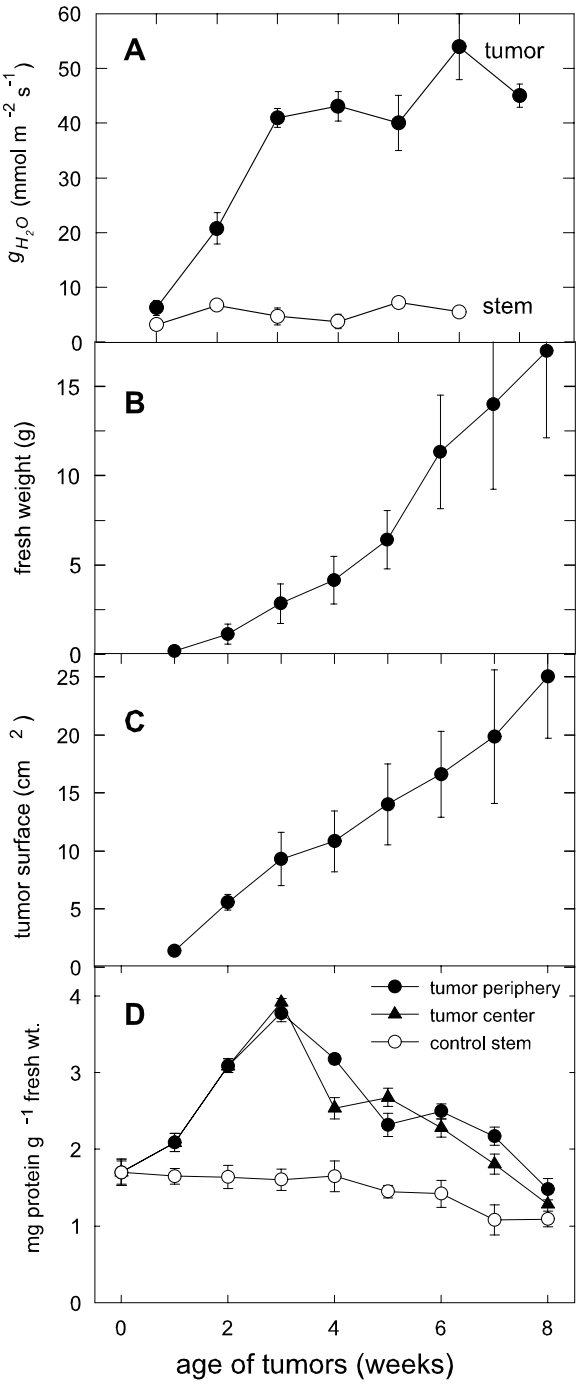

Figure 2. g_{H2O} and growth of tumors after infection of castor bean hypocotyls with *A. tumefaciens* C58. A, Increase of g_{H2O} during tumor growth, related to the irregular tumor surface; mean values ± SE (n = 3–5). B, Increase of tumor fresh weight during its development over 8 weeks; mean values ± SE (n = 9–48). C, Linear increase of the irregular tumor surface (n = 9–17). D, Protein concentration during tumor growth of peripheral cell layers (1–2 mm), the center, and control stem; mean values ± SE (n = 3–48).

Impact of Tumor Transpiration

Key features of development in the large, *A. tumefaciens*-induced tumors of castor bean were shown here to be ethylene dependent (Fig. 1, A–E), as observed for *Never ripe* tomatoes (Aloni et al. 1998) and furthermore were shown to arise from direct effects of tumor ethylene biosynthesis (Fig. 1E). Ethylene-insensitive *Never ripe* tomato plants do not develop tumors upon infection with virulent agrobacteria despite integration and expression of the T-DNA oncogenes for auxin and cytokinin biosynthesis (Aloni et al., 1998). An additional line of evidence for essential ethylene responses is provided here by application of the ethylene synthesis inhibitor AVG to the tumor alone, which suppressed not only its own development, but also epinastic responses of neighboring leaves (Fig. 1, A and D). Vascularization was also completely inhibited and hence tumor growth (Fig. 1, D and E). Without ethylene inhibitors, tumor bundles were well-developed, with phloem and xylem functionally connected to that of the host stem (Aloni et al., 1995; Schurr et al., 1996). Cuticular rupture was also ethylene dependent and was found here to coincide with marked increases in water flow. Together, these changes in vascularization and epidermal alterations thus constitute ethylene-induced mechanisms ensuring continuous water supply to the tumor.

Because tumor proliferation also leads to dwarf size of the host shoot (Fig. 1A), the gall constriction hypothesis was investigated to determine the extent to which water competition by the tumor contributes to these effects. Schurr et al. (1996) provided the first semiquantitative data of a relationship between the water regime of the tumor, vascularization, cuticle, and stomata development. Now, we have thoroughly quantified g_{H2O} during tumor development and related this to the highly irregular tumor surface (Fig. 1A, inset).

In the light, J_{H2O} for a given leaf area of uninfected castor bean plants was about seven times that of tumors on plants of the same age (Table I), whereas leaf transpiration rate dropped to one-half that of tumors in the dark. A further comparison of J_{H2O} for the total transpiring surfaces of a 3-week-old tumor (10 cm^2 surface) with a host plant with five leaves (400 cm^2 surface each leaf) revealed that, in the light, J_{H2O} of the leaves was about 1,470 times greater than that of the tumor. For a shoot with five leaves, comparative transpiration by the tumor would thus be negligible. However, the transpiration rate for leaves of tumor-infected plants is typically only 10% of that for noninfected plants (Veselov et al., 2003), due to the induction of ABA production by tumor-emitted ethylene (Mistrik et al., 2000; Veselov et al., 2003). Ethylene-induced closure of stomata due to ABA accumulation has been reported by Mayak and Halevy (1972), Pallas and Kays (1982), and Taylor and Gunderson (1988). In addition, ethylene and ABA signaling are partly overlapping and interfering (Beaudoin et al., 2000; Ghassemian et al., 2000; Hansen and Grossmann, 2000).

Table I. g_{H2O} *and* J_{H2O}

Three-week-old tumors and leaves of uninfected castor bean plants of the same age measured during the light and dark period (each for 10 h). Mean values ± SE (*n*).

	Tumor		Leaf	
	Light Period	Dark Period	Light Period	Dark Period
	mmol m^{-2} *s*$^{-1}$			
g_{H2O}	34.8 ± 3.7 (6)	28.2 ± 4.2 (4)	361.7 ± 26.5 (3)	12.3 ± 0.8 (3)
J_{H2O}	0.54 ± 0.06 (6)	0.38 ± 0.06 (4)	3.97 ± 0.62 (3)	0.21 ± 0.02 (3)

In conclusion, the amount of water loss through the tumor surface was considerably lower than the sum of water loss through the leaves of uninfected control plants. Ethylene emission from the tumor on ABA induction in the host leaves, leading to drastic stomata closure (Veselov et al., 2003), resulted in a 90% diminished transpiration rate, which is still about 150 times that of the tumor. But this phytohormone signaling from the tumor to the host shoot has to be regarded as the crucial regulating step in the water regime of the host plant with substantial consequences for nutrient partitioning between the host shoot and the tumor.

Tumor Suc Demand and Suc-Cleaving Enzymes

Substantial demand for Suc import includes high respiratory activity (Fig. 3). The redox potential in plant tumor tissue is relatively low (Beardsley, 1972) and typical of the reduced state often found in growing tissue. In addition, previous 3-(4,5-dimethylthiazolyl)-2,5-diphenyl-tetrazolium bromide staining revealed elevated production of cellular NADH indicative of rapid respiration and glycolysis (Wächter et al., 1999; Schwalm et al., 2003). The C-cost of this respiration during tumor development was quantified here by continuous measurement of net CO_2 release during tumor growth. Tumor emission rates were up to 18-fold those of the uninfected stem (Fig. 3). The sigmoidal increase in J'_{CO2} correlated well with growth (Fig. 2B) and indicated a high demand for Suc import.

In young tumors, the activity of vacuolar, but not CWIN, was consistent with a major role in the direct import of symplastically transported Suc (Pradel et al., 1996; 1999). Previous work showed that GFP-

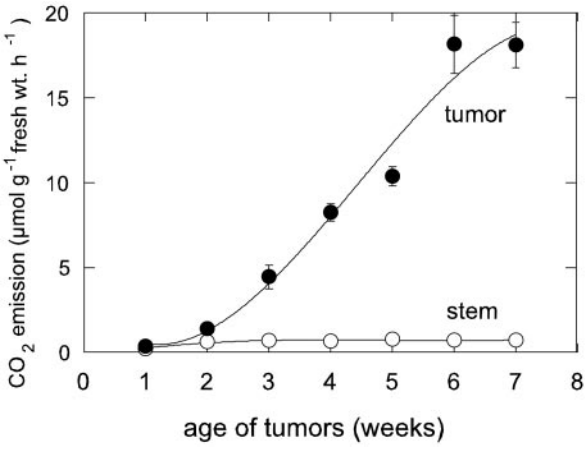

Figure 3. Sigmoidal increase of net CO_2 emission from the tumors during the light period; mean values ± SE (*n* = 3–6).

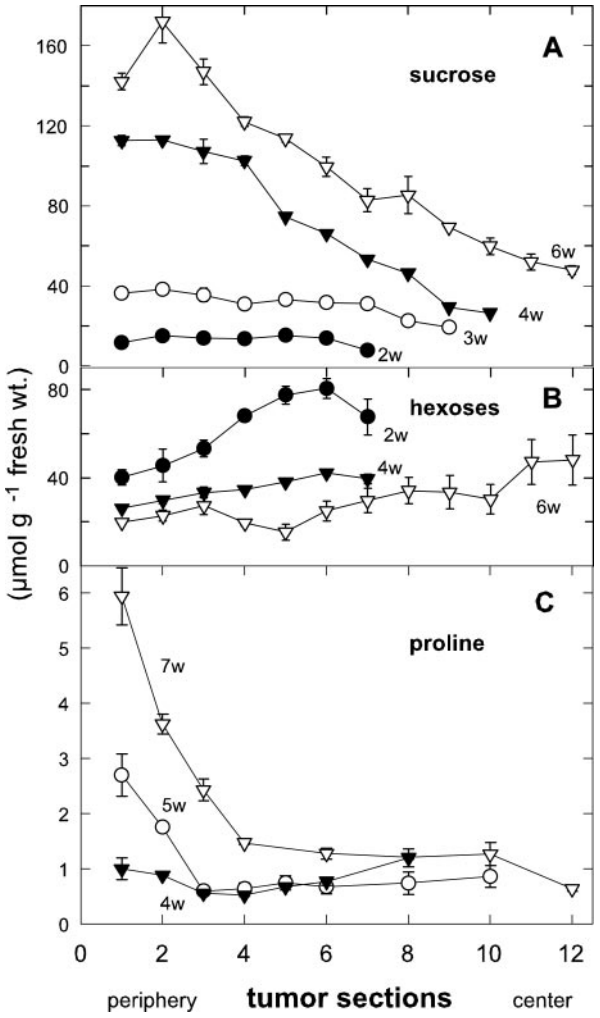

Figure 4. Concentration gradients of Suc, hexoses, and Pro from the periphery to the center in castor bean tumors. A, Decreasing Suc concentration gradient and increase in Suc concentration with tumor age (w, weeks p.i.). B, Increasing hexose concentration gradient and decrease of hexose concentration with tumor age. C, Rapidly decreasing Pro concentration gradient and increase of Pro concentration with tumor age; mean values ± SE (*n* = 3–6).

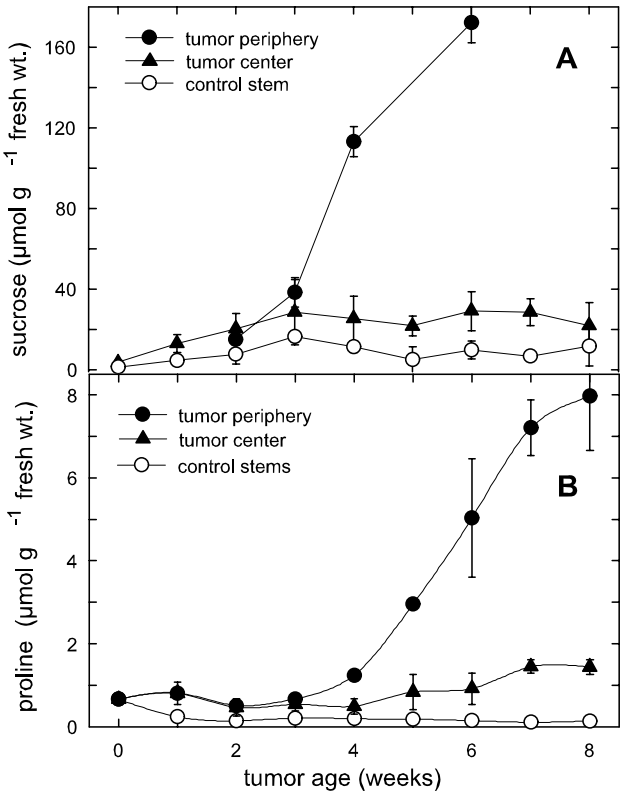

Figure 5. Suc and Pro concentration and spatial distribution in castor bean tumors. Late increase of (A) Suc and (B) Pro concentration in the periphery during tumor development; mean values ± SE (n = 3–6).

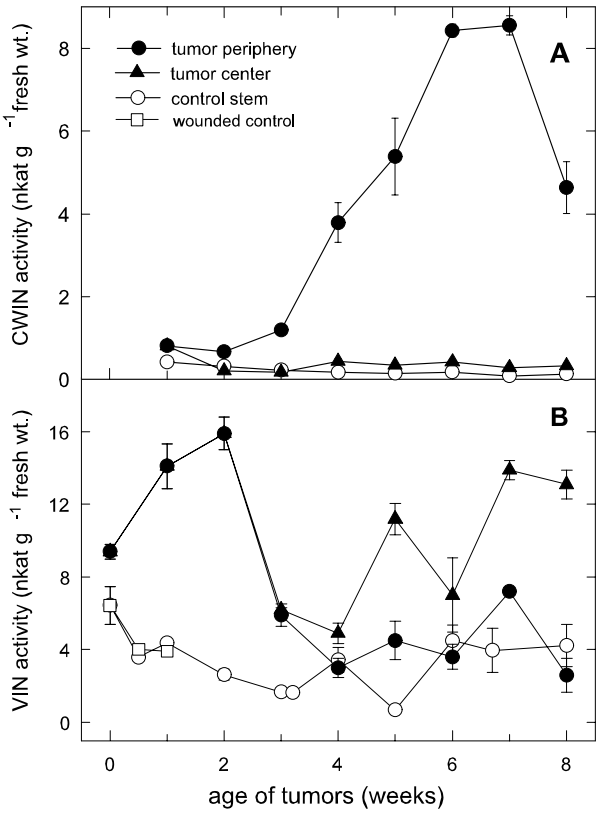

Figure 6. Activity and spatial distribution of Suc-cleaving enzymes during the development of castor bean tumors. A, Acid CWIN activity in the periphery and center of tumors and in the control stem. B, Vacuolar acid invertase (VIN) activity in the periphery and center of the tumors and in unwounded and wounded control stems; mean values ± SE (n = 3–6).

labeled potato virus X and fluorescent dyes like Lucifer Yellow CH and carboxyfluorescein were imported symplastically from the host leaves via the phloem into tumor parenchyma cells across the numerous plasmodesmata (Pradel et al., 1996, 1999). Hence, the smaller Suc molecule could also be distributed symplastically to sites of cleavage by VIN and SuSy without encountering CWIN. This independence of early import from CWIN activity is further supported by the present results (Fig. 6A), showing that CWIN activity did not rise until relatively late in tumor development.

Early tumor growth was also characterized by a close relationship between VIN (Fig. 6B) and accumulation of free auxin and cytokinins in castor bean tumors during their first 2 weeks of development (Veselov et al., 2003). Also, sites of VIN activity (Fig. 6B) corresponded to defined patterns of localization for both phytohormone types (identified by monoclonal mouse hybridoma antibodies) at the tumor center, around and within developing vascular bundles, and to a lesser degree, in the tumor periphery (Veselov et al. 2003). Comparable relationships were not observed for CWIN (Fig. 6A).

Analysis of later tumor growth revealed distinctive features of CWIN regulation in this system. First, it was not induced during periods of either auxin or cytokinin production by the young tumor. The lack of auxin induction is consistent with the repression of some sugar response elements by auxin (DeWald et al., 1994), but the nonresponsiveness of CWIN to cytokinins contrasts with its induction by them in cell cultures (Ehness and Roitsch, 1997). Second, CWIN was up-regulated in the presence of elevated Suc and

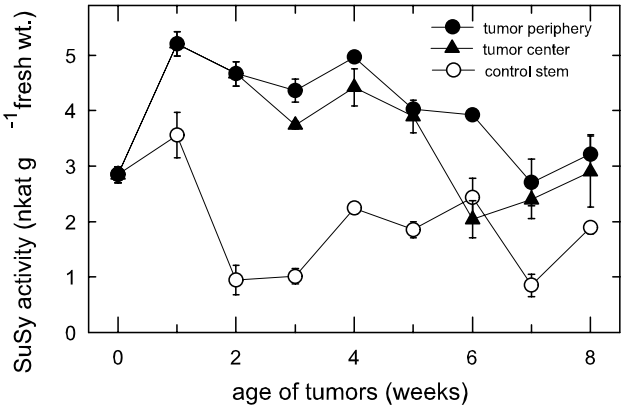

Figure 7. Activity and spatial distribution of SuSy during tumor development. SuSy activity in the periphery and center of tumors and in the control stem; mean values ± SE (n = 3–6).

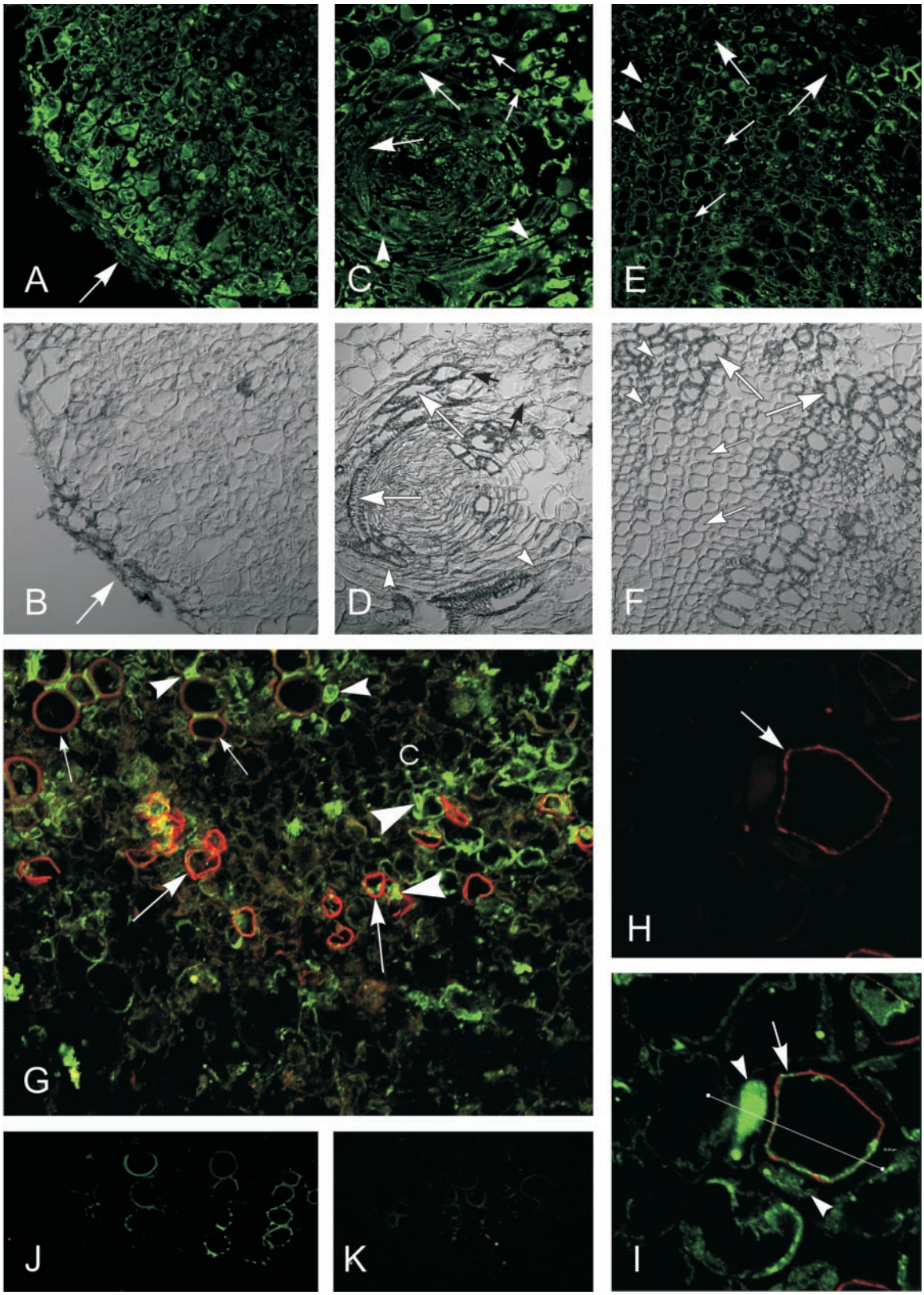

Figure 8. Immunolocalization of SuSy in 2-week-old castor bean tumor sections with specific polyclonal antibodies against *Sh1* and *Sus1* proteins; secondary antibodies were labeled with the green Alexa 488 chromophore, viewed by confocal laser scanning microscopy (CLSM). A, The highest fluorescence label was localized in the tumor periphery (arrow), decreasing to

(*Legend continues on facing page.*)

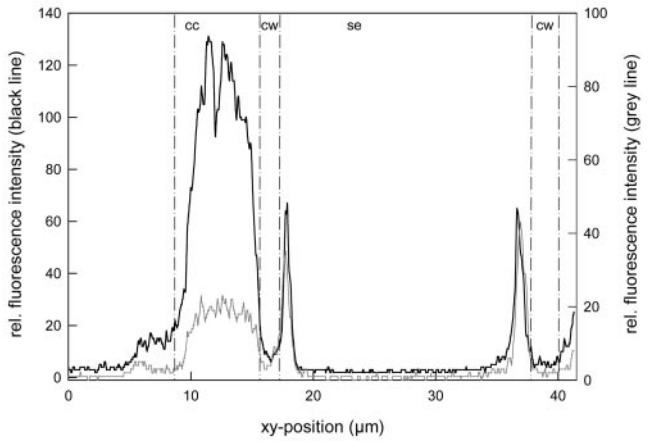

Figure 9. CLSM fluorescence intensity measurements of Alexa 488-labeled SuSy (*Sus1*/*Sh1*) antibodies (black line) and Alexa 568-labeled PM H^+-ATPase antibody clone 44B8A1 (gray line) along the straight line, from left to right, indicated in Figure 8I; cc, companion cell; cw, cell wall; se, sieve element.

ABA. The timing and sites of enzyme activity coincided with maximal Suc and Pro concentrations during tumor development (Figs. 5 and 6), highest transpiration rates in older tumors (Fig. 2A), and a late maximum in ABA synthesis (Veselov et al., 2003). These data suggest that with increasing tumor age, cell water stress increases concurrent with the accumulation of osmotically protective substances. Although hexoses in the vacuole can aid turgor maintenance under moderate stress, Suc in particular is a superior cytoplasmic osmoprotectant under moderate stress (Hochachka and Somero, 2002), where its presence in the cytoplasm can aid protection of membrane constituents without altering metabolic balance and signals to the degree that hexoses do. Suc can rise to high concentrations throughout the cell interior if invertase activity is repressed or restricted to the cell wall space. High-Suc accumulation is thus compatible with CWIN activity, and Suc can even protect the enzyme against its proteinaceous inhibitor (Sander et al., 1996). Some CWIN genes are also induced by extracellular sugars (LaLonde et al., 1999). ABA involvement is also possible for induction of CWIN in the periphery of maturing tumors, because specific and distinct immunolocalization of ABA was visible in the outermost cell layers (Fig. 1H). That at least some invertases respond directly to ABA (K.E. Koch, unpublished data) correlates well with the early maximum of VIN in the tumor center (Fig. 6B), together with the first peak in ABA accumulation (Veselov et al., 2003) and a distinct ABA-specific immunofluorescence in the tumor center around the vascular bundles in 3-week-old tumors (Fig. 1, F–I). Invertases can be up-regulated by drought stress in vegetative tissues (Pelleschi et al., 1999; Kim et al., 2000). Recent evidence also indicates common paths for ABA and sugar signals (Rolland et al., 2002; Leon and Sheen, 2003) and/or ABA enhancement of sugar sensing (Smeekens, 2000; Rook et al., 2001).

These data raise questions about the seemingly enigmatic role of CWIN in a system with an intact symplastic transport path and high levels of Suc accumulation. However, symplastic continuity does not prevent movement of Suc into the cell wall space, and varying degrees of apoplastic transfer can often occur. When it does, a defined fraction of the translocated Suc can be cleaved by CWINs if they are present and active, as indicated for the periphery of maturing tumors (Fig. 6A). Because this extracellular process is isolated from the greater mass of cellular cytoplasm and vacuole, high concentrations of Suc can accumulate in the same cells and tissues. Under these conditions, CWIN can contribute to localized apoplastic import as well as adjustment of osmotically active hexose concentrations immediately outside cells. Both actions could favor establishment of descending turgor gradients so necessary for Suc import. Control of turgor gradients could be invaluable in a rapidly transpiring structure like the castor bean tumors, where water potential and solute flow could vary markedly during a diurnal period and from cell to cell.

Finally, a key developmental role may be played by the CWIN at the tumor periphery, because even sym-

Figure 8. (Legend continued from facing page) the tumor center. B, Same as A in DIC mode. C, Immunofluorescence label of SuSy in a tumor-typical circular vascular bundle in xylem parenchyma cells (small arrows) associated with the circular vessels (large arrows) and in companion cells (arrowheads) of sieve elements. D, Same as C in DIC mode. E, Immunofluorescence label of SuSy in the pathological xylem of the tumor/host stem interface, in particular in the xylem parenchyma cells (arrowheads), adjacent to the vessels (large arrows), but pathological multiseriate rays (thin arrows) without fluorescent label. F, Same as E in DIC mode. G, Overview of phloem and xylem (small arrows, weak autofluorescence of vessels) and cambium (c) in a control stem with specific immunolabeling with anti-PM H^+-ATPase monoclonal mouse hybridoma antibodies (red Alexa 568 chromophore) of the PM H^+-ATPase in the plasma membrane of sieve elements (large arrows) and green immunofluorescence label of SuSy predominantly in phloem companion cells (large arrowheads), in sieve elements, and in xylem parenchyma cells (small arrowheads). H, Specific immunolabeling (red Alexa 568 chromophore) of the PM H^+-ATPase (arrow) in the plasma membrane of sieve elements in a control stem. I, Same section showing double immunolabeling (green Alexa 488) of SuSy in companion cells (arrowheads) and the thin cytoplasmic layer and of the PM H^+-ATPase (red Alexa 568 chromophore) in sieve elements (arrow). Straight line CLSM fluorescence intensity measurement, from left to right (see Fig. 9). J and K, Control tumor sections incubated without primary antibodies showing only autofluorescence of lignified vessels with 1% (w/v) mouse IgG, labeled with the secondary goat-anti-mouse Alexa 488 antibody (J) and with 1% (w/v) BSA, labeled with the secondary goat-anti-rabbit Alexa antibody (K); viewed with CLSM, the amplification of the photomultiplier was set to 760 throughout. Bars in A through G, J, and K = 80 μm; in H and I = 20 μm.

plastical intact systems such as carrot (*Daucus carota*) plantlets, can require CWIN for normal separation of expanding leaves (Sturm et al., 1995; Sturm and Tang, 1999). In addition, restriction of invertase action to the cell wall compartment may be critical to the increase of Suc/hexose ratios recently implicated in signals to genes for maturation and desiccation tolerance (Wobus and Weber, 1999). Both of the above functions for CWIN could be invoked during final phases of tumor development.

SuSy distribution in the tumor is compatible with three new aspects of its function, two of these with special implications for the developing castor bean tumor. The first of these was the extent of its labeling along a gradient toward the periphery (Fig. 8A). SuSy action in these cells would have been invaluable to a dual role in facilitating both Suc import and high-volume solution flow. Cytoplasmic action of SuSy would complement that of CWIN in maintaining low turgor at the terminal end of the transport path by rapid carbohydrate metabolization. This, plus the osmoprotective advantage of an endogenous, high-Suc environment in the cytoplasm of these cells (Figs. 4 and 5), would be compatible with a SuSy-based path for respiration (Huber and Akazawa, 1986). The latter would also favor biosynthesis of cell wall and/or pectic materials in cells at the tumor surface (F. Baluška, unpublished data).

The second new aspect of SuSy localization was its identification in the distinctive xylem parenchyma cells of the tumor (Fig. 8, C and G). They are strategically positioned adjacent to large vessel elements, where they can readily function in mineral nutrient uptake. Furthermore, they lie at sites where they can mediate xylem-to-phloem transfer of nutrients. Immunolocalization data for these key cells in the present system support a mechanistic role for SuSy in acquisition and handling of the inorganic nutrients so critical to tumor establishment.

Finally, the clarity of SuSy localization achieved in this system allowed a resolution of its role in phloem function, regardless of position in tumor or control tissue (Figs. 8I and 9). Previous work had established that SuSy promoters are active in phloem (Yang and Russell, 1990) and that companion cells in particular are sites of high expression (Nolte and Koch, 1993). However, work here showed that SuSy was also present in the thin layer of cytoplasm that lines sieve elements in the phloem.

This SuSy localization in sieve elements is an important extension of earlier research in several ways. First, data now indicate that the previously envisioned role of SuSy in contributing UDP-Glc to biosynthesis of callose for protective plugging of phloem (Nolte and Koch, 1993; van Bel, 2003) can occur in the same cells where the callose is produced. This initial model proposed a pivotal position for SuSy in the balance between callose biosynthesis and respiration (Nolte and Koch, 1993). Adenylate analyses of phloem exudates (Geigenberger et al., 1993) further indicated that although SuSy itself was not detectable, its bound or near-by activity would have been operating under conditions compatible with maintenance of high-Suc concentrations. However, direct evidence was lacking for presence of SuSy in the sieve elements per se. Second, the immunolocalization of sieve element SuSy close to plasma membrane H^+-ATPases shown here also suggests a fine-tuned regulation between energy supply and demand. Third, the SuSy-based respiratory path could provide an on-site avenue for conversion of Suc to ATP in the cytoplasm of sieve elements and thus make it readily available for localized instances and rapid demand, despite the lack of a normal mitochondrial population in these cells. Data provided here show the physical localization to support all three of these proposed roles for SuSy in the sieve elements.

In conclusion, vascularization and cuticular rupture, both central to ethylene-dependent establishment of tumors, were appraised here relative to their functional significance for water and sugar transfer. Data support the following advances.

For water flow: (a) A striking relationship was revealed between the timing of cuticular rupture in young tumors and dramatic increases in the water flow essential for delivery of inorganic nutrients. (b) Assessment of the gall constriction hypothesis (Aloni et al., 1995) indicated direct effects of tumor water loss on shoot growth would be minimal and largely nocturnal.

For sugar utilization and import: (a) Successful tumors accumulated first hexoses and then Suc in a change that often alters sugar signals from those favoring cell division to those for maturation and desiccation tolerance. Direct effects of this shift would also aid initial tumor expansion, and later gradients in turgor and osmoprotection. (b) Tumor development also involved a transition from VIN, as a mediator of symplastic import and hexose concentration in young tumors, to CWIN, positioned to maintain descending turgor gradients in the periphery of older tumors. Correlation of both VIN and CWIN with ABA concentration gradients is in line with recent evidence for common paths for sugar and ABA signals. (c) Three new roles for SuSy were implicated, including: (i) import and respiration in the osmoprotective, high-Suc cytoplasm at the tumor periphery, (ii) mineral nutrient uptake and transfer by specific xylem parenchyma cells present in successfully established tumors, and (iii) functioning of phloem, not only in companion cells, but also in the unique interior of sieve elements.

MATERIALS AND METHODS

Plant Material and Tumor Induction

Castor bean (*Ricinus communis* L. var *gibsonii* cv Carmencita; Walz Samen, Stuttgart, Germany) was grown and infected with *Agrobacterium tumefaciens*

C58 as described in detail previously (Pradel et al., 1996). After appearance of the first leaves, the plant hypocotyls were wounded with a razor blade 10 mm below the cotyledons and were inoculated with bacterial pellet.

Determination of the Tumor Surface

To compare the transpiration rate of tumors with that of leaves, the highly irregular surface of the tumors (Fig. 1, A and B) had to be determined. A plastic polymer (Xantopren, Haraeus Kulzer, Dormagen, Germany) was spread over the tumor surface. The mixture of the activator (8 drops) and Xantopren (1 g) became elastic after a few minutes and was removed, giving the shape of the irregular surface. The slightly sticky impression was covered with a layer of glass balls (0.06–0.46 mm in diameter; Sodaklarglas, Wenzel, Heidelberg). The ratio of the difference in weight of the Xantropren-impression with and without glass balls to the weight of the glass ball layer of a known surface yielded the tumor surface. The surface of the leaves was scanned and calculated by the NIH Image software (developed at the United States National Institutes of Health and available on the Internet at http://rsb.info.nih.gov/nih-image), taking into account that castor bean leaves are amphistomatic.

Cuticle Staining

Cuticles of tumor cross sections were stained red for 10 s in Sudan III solution (0.2 g dissolved in 100 mL of isopropanol and 100 mL of distilled water). The sections were viewed in glycerol with an Aristoplan epifluorescence microscope (Leica, Bensheim, Germany). Micrographs were reproduced from color slides taken with an Orthomat E camera system (Leica) on Kodak Ektachrome Elite 100 (Eastman Kodak, Rochester, NY).

AVG Treatment

To investigate the influence of ethylene on tumor growth and vascularization, the ethylene synthesis inhibitor AVG was applied at the site of infection 1 d after inoculation with bacteria. A Terostat funnel (Teroson, Heidelberg) was maintained filled with 10 μM aqueous AVG solution or distilled water as control. After 3 weeks, cross sections from tumor and host stem tissue were stained with toluidine blue (0.05%) and were viewed with a stereo photomacroscope (M 400, Wild, Heerbrugg, Switzerland). The micrographs were reproduced from Kodak Ektachrome 64T color slides.

Gas Exchange Measurements

Net CO_2 emission of uninfected stems and tumors was measured with a minicuvette system (Walz, Effeltrich, Germany) as described previously (Rascher et al., 1998). CO_2 emission and g_{H2O} were measured in a climate-regulated chamber of the local phytotron. Net CO_2 emission and transpiration of 1- to 7-week-old tumors and of leaves of 3-week-old uninfected plants were recorded every 5 h. Air temperature and humidity (set at 60% $\pm$ 5%) were measured and controlled inside the gas exchange cuvette, which enclosed the leaf, the uninfected stem, or the attached tumor together with the plant stem. Irradiance (photosynthetic photon flux density) was measured in the range of 400 to 700 nm using a quantum sensor (LI-COR, Lincoln, NE) and was set to 110 $\pm$ 10 μmol m^{-2} s^{-1}. The J'_{CO2} and g_{H2O} as well as the J_{H2O} were calculated according to Farquhar and Sharkey (1982).

Suc-Cleaving Enzymes

Either randomized samples of the whole tumor or 2-mm-thick tangential tumor sections and samples of the control stem (100–500 mg) were harvested, rapidly frozen in liquid nitrogen, and homogenized in Teflon capsules with a micro-dismembrator (Braun, Melsungen, Germany).

For the determination of acid CWIN and soluble VIN, the frozen powder was suspended in 5 mL of buffer containing 100 mM MOPS, 250 mM sorbitol, 10 mM KCl, 10 mM $MgCl_2$, 1 mM phenylmethylsulfonyl fluoride, 3% (w/v) polyvinylpyrrolidone (for CWIN) or 5% (w/w) polyvinylpolypyrrolidone (for VIN), and 2 mM dithiothreitol (DTT), at pH 6. After centrifugation, the pellet was resuspended in the buffer without polyvinylpyrrolidone. After washing three times with distilled water, the pellet was resuspended for the CWIN assay in hydrolyzing buffer (20 mM triethanolamine hydrochloride, 6.7 mM citric acid, and 20 mM Suc, pH 4.6) and incubated at 37°C for 30 min; the supernatant was used for the VIN assay. The reaction was stopped by heating at 100°C for 5 min. After centrifugation, the released Glc was determined in the supernatant by the dianisidin method (Fermognost, Feinchemie Sebnitz, Germany).

SuSy was determined according to Dancer et al. (1990) as the amount of UDPG released during 20 min of incubation with a desalted extract by the stoichiometric production of NADH (at 340 nm) in the presence of UDP-Glc dehydrogenase after extraction with buffer (extraction buffer: 50 mM HEPES, 12 mM $MgCl_2$, 1 mM EDTA, 1 mM EGTA, pH 7.4, 1 mM benzamidine, 1 mM ϵ-aminocapronic acid, 2 mM DTT, 0.1% [v/v] Triton X-100, 1 mM phenylmethylsulfonyl fluoride, and 20 mg of polyvinylpolypyrrolidone). Extracts were purified over a Sephadex G-25 column in desalting buffer (50 mM HEPES, 12 mM $MgCl_2$, and 2 mM DTT, pH 7.4). The incubation buffer contained 20 mM HEPES, pH 7.0, 100 mM Suc, and 4 mM UDP. The reaction was carried out in buffer containing 165 mM Gly, 4 mM $MgCl_2$, 0.25 mM NAD, pH 8.7, and 0.07 units of UDP-Glc dehydrogenase.

Suc, Hexoses, Pro, and Protein

The metabolites were determined after methanol extraction (80%). Suc was determined colorimetrically at 490 nm, hexoses at 535 nm according to Büttner et al. (1985), and Pro at 515 nm according to Troll and Lindsley (1955) with ninhydrin and upon partitioning in toluene. Protein concentration was determined with acid amido black at 620 nm according to Popov et al. (1975).

Immunolocalization of SuSy and ABA

For immunolocalization 2- and 3-week-old tumor samples were fixed for 4 h at 22°C with 4% (w/v) paraformaldehyde or *N*(3-dimethylethylaminopropyl)-*N*-ethylcarbodiimide-HCl in 0.1× phosphate-buffered saline (PBS) containing 0.1% (v/v) Triton X-100 (0.1× PBS: 13.7 mM NaCl, 0.15 mM KH_2PO_4, 0.79 mM Na_2HPO_4, and 0.27 mM KCl, pH 7). After dehydration with a graded series of ethanol at 22°C, the tissue was imbedded overnight in Steedman's wax, a polyester with a low melting point (PEG 400 distearate in hexadecanol 9:1 [w/w]). Cross sections of 12 μm thickness were prepared with a cryomicrotome (Cryocut CM 3050, Leica) and collected on poly-L-Lys coated slides. The sections were dewaxed with decreasing ethanol concentrations, rinsed with 0.1× PBS, incubated with buffer for 30 min, and with 100% (v/v) methanol for 10 min at −20°C. For immunolabeling, the sections were incubated overnight with the polyclonal rabbit anti-SuSy serum, raised against a combination of *Sh1* and *Sus1* gene products extracted from whole maize (*Zea mays*) kernels (W64A × 182E) 22 d after pollination (Koch et al., 1992), and diluted 1:500 in 1% (w/v) BSA solution. For ABA immunolocalization, mouse monoclonal hybridoma antibodies raised against ABA-BSA conjugate (ABA-15-I-C-5; Agdia-Phytodetek/Linaris, Wertheim-Bettingen, Germany) were used with high specificity for 2-cis-(S)-ABA and with cross-reactivity of less than 1 or 0 against 12 ABA structurally related compounds (Weiler, 1982). For SuSy labeling the green fluorescent Alexa conjugate (488 goat anti-rabbit IgG, H + L; Molecular Probes, Göttingen, Germany) was used as secondary antibody, diluted 1:200 with 1% (w/v) BSA in 0.1× PBS and applied for 2 h at 22°C. For simultaneous labeling of the plasma membrane (PM) H^+-ATPase in sieve elements, the sections were subsequently incubated with the mouse monoclonal PM H^+-ATPase antibody clone 44B8A1 in hybridoma supernatant (Langhans et al., 2001). Here, the red fluorescent Alexa conjugate (568 goat anti-mouse IgG, H+L) was used as secondary antibody. For ABA labeling, the green fluorescent Alexa conjugate (488 goat anti-mouse IgG, H+L) or the red fluorescent Alexa conjugate (568 goat anti-mouse IgG, H+L) was used. After immunolabeling, the sections were mounted on slides in buffer. Control sections were incubated without primary antibodies either with 1% (w/v) BSA or with 1% (w/v) rabbit serum (Sigma-Aldrich, St. Louis) and did not show secondary antibody-caused fluorescence (Figs. 1M and 8, J and K). About 300 sections were viewed with a confocal laser scanning microscope (TCS SP-MP, DM IBRE inverted microscope, Leica). Fluorescence was excited with 488-nm light (emission 515–525 nm) or 568-nm light (emission 600–615 nm) using a 50-mW krypton/argon laser. Further details have been described recently (Langhans et al., 2001; Aloni et al., 2003; Veselov et al., 2003).

Distribution of Materials

Upon request, all novel materials described in this publication will be made available in a timely manner for noncommercial research purposes, subject to the requisite permission from any third-party owners of all parts of the material. Obtaining any permission will be the responsibility of the requestor.

ACKNOWLEDGMENTS

We thank Sylvia Lenz, Ingrid Scheel (Darmstadt University of Technology) and Heike Weiner (University of Heidelberg) for valuable technical assistance and Prof. Ulrich Lüttge (Darmstadt University of Technology) for support and critical discussions.

Received June 5, 2003; returned for revision July 14, 2003; accepted July 27, 2003.

LITERATURE CITED

Aloni R, Pradel KS, Ullrich CI (1995) The three-dimensional structure of vascular tissues in *Agrobacterium tumefaciens*-induced crown galls and in the host stems of *Ricinus communis* L. Planta **196:** 597–605

Aloni R, Schwalm K, Langhans M, Ullrich CI (2003) Gradual shifts in sites of free-auxin production during leaf-primordium development and their role in vascular differentiation and leaf morphogenesis in *Arabidopsis*. Planta **216:** 841–853

Aloni R, Wolf A, Feigenbaum P, Avni A, Klee HJ (1998) The *Never ripe* mutant provides evidence that tumor-induced ethylene controls the morphogenesis of *Agrobacterium tumefaciens*-induced crown galls on tomato stems. Plant Physiol **117:** 841–849

Beardsley RE (1972) The inception phase in the crown gall disease. Prog Exp Tumor Res **15:** 1–75

Beaudoin N, Serizet C, Gosti F, Giraudat J (2000) Interactions between abscisic acid and ethylene signaling cascade. Plant Cell **12:** 1103–1115

Büttner G, de Fekete MAR, Vieweg GH (1985) Changes in fructan content in developing barley caryopses. Angew Bot **59:** 171–177

Dancer J, Hatzfeld WD, Stitt M (1990) Cytosolic cycles regulate the turnover of sucrose in heterotrophic cell-suspension cultures of *Chenopodium rubrum*. Planta **182:** 223–231

DeWald DB, Sadka A, Mullet JE (1994) Sucrose modulation of soybean *Vsp* gene expression is inhibited by auxin. Plant Physiol **104:** 439–444

Ehness R, Roitsch T (1997) Co-ordinated induction of mRNAs for extracellular invertase and a glucose transporter in *Chenopodium rubrum* by cytokinins. Plant J **11:** 539–548

Farquhar GD, Sharkey TD (1982) Stomatal conductance and photosynthesis. Annu Rev Plant Physiol **33:** 317–345

Geigenberger P, Langenberger P, Wilke I, Heineke D, Heldt HW, Stitt M (1993) Sucrose is metabolised by sucrose synthase and glycolysis within the phloem complex of *Ricinus communis* L. seedlings. Planta **190:** 446–453

Ghassemian M, Nambara E, Cutler S, Kawaide H, Kamiya Y, McCourt P (2000) Regulation of abscisic acid signaling by the ethylene response pathway in *Arabidopsis*. Plant Cell **12:** 1117–1126

Hansen H, Grossmann K (2000) Auxin-induced ethylene triggers abscisic acid biosynthesis and growth inhibition. Plant Physiol **124:** 1437–1448

Hochachka PW, Somero GN (2002) Biochemical Adaptation: Mechanism and Process in Physiological Evolution. Oxford University Press, New York

Huber SC, Akazawa T (1986) A novel sucrose synthase pathway for sucrose degradation in cultured sycamore cells. Plant Physiol **81:** 1008–1013

Kim J-Y, Mahe A, Brangeon J, Prioul J-L (2000) A maize vacuolar invertase, IVR2, is induced by water stress: organ/tissue specificity and diurnal modulation of expression. Plant Physiol **124:** 71–84

Koch KE (1996) Carbohydrate-modulated gene expression in plants. Annu Rev Plant Physiol Plant Mol Biol **47:** 509–540

Koch KE, Nolte KD, Duke ER, McCarty DR, Avigne WT (1992) Sugar levels modulate differential expression of maize sucrose synthase genes. Plant Cell **4:** 59–69

Kutschera U, Bahrami M, Grotha R (2000) Sucrose metabolism during *Agrobacterium tumefaciens*-induced tumor growth in sunflower hypocotyls. J Plant Physiol **157:** 1–6

LaLonde S, Boles E, Hellmann H, Barker L, Patrick JW, Frommer WB, Ward JM (1999) The dual function of sugar carriers: transport and sugar sensing. Plant Cell **11:** 707–726

Langhans M, Ratajczak R, Lützelschwab M, Michalke W, Wächter R, Fischer-Schliebs E, Ullrich CI (2001) Immunolocalization of plasmamembrane H^+-ATPase and tonoplast-type pyrophosphatase in the plasma membrane of the sieve element-companion cell complex in the stem of *Ricinus communis* L. Planta **213:** 11–19

León P, Sheen J (2003) Sugar and hormone connections. Trends Plant Sci **8:** 110–116

Malsy S, van Bel AJE, Kluge M, Hartung W, Ullrich CI (1992) Induction of crown galls by *Agrobacterium tumefaciens* (strain C 58) reverses assimilate translocation and accumulation in *Kalanchoë daigremontiana*. Plant Cell Environ **15:** 519–529

Mayak S, Halevy AH (1972) Interrelationships of ethylene and abscisic acid in the control of rose petal senescence. Plant Physiol **50:** 341–346

Mistrik I, Pavlovkin J, Wächter R, Pradel KS, Schwalm K, Hartung W, Mathesius U, Stöhr C, Ullrich CI (2000) Impact of *Agrobacterium tumefaciens*-induced stem tumors on NO_3^- uptake in *Ricinus communis*. Plant Soil **226:** 87–98

Nolte KD, Koch KE (1993) Companion-cell specific localization of sucrose synthase in zones of phloem loading and unloading. Plant Physiol **101:** 899–905

Pallas JE, Kays SJ (1982) Inhibition of photosynthesis by ethylene: a stomatal effect. Plant Physiol **70:** 598–601

Pavlovkin J, Okamoto H, Wächter R, Läuchli A, Ullrich CI (2002) Evidence for high activity of xylem parenchyma and ray cells in the interface of host stem and *Agrobacterium tumefaciens*-induced tumours of *Ricinus communis*. J Exp Bot **53:** 1143–1154

Pelleschi S, Guy S, Kim J-Y, Pointe C, Mahe A, Barthes L, Leonardi A, Prioul JL (1999) Ivr2, a candidate gene for a QTL of vacuolar invertase activity in maize leaves: gene-specific expression under water stress. Plant Mol Biol **39:** 373–380

Popov N, Schmitt M, Schulzeck S, Matthies H (1975) Eine störungsfreie Mikromethode zur Bestimmung des Proteingehaltes in Gewebehomogenaten. Acta Biol Med Ger **34:** 1441–1446

Pradel KS, Ullrich CI, Santa Cruz S, Oparka KJ (1999) Symplastic continuity in *Agrobacterium tumefaciens*-induced tumours. J Exp Bot **50:** 183–192

Pradel SK, Rezmer C, Krausgrill S, Rausch T, Ullrich CI (1996) Evidence for symplastic phloem unloading with concomitant high activity of acid cell wall invertase in *Agrobacterium tumefaciens*-induced plant tumors. Bot Acta **109:** 397–404

Rascher U, Blasius B, Beck F, Lüttge U (1998) Temperature profiles for the expression of endogenous rhythmicity and arrhythmicity of CO_2 exchange in the CAM plant *Kalanchoë daigremontiana* can be shifted by slow temperature changes. Planta **207:** 76–82

Rezmer C, Schlichting R, Wächter R, Ullrich CI (1999) Identification and localization of transformed cells in *Agrobacterium tumefaciens*-induced plant tumors. Planta **209:** 399–405

Roitsch T, Ehness R (2000) Regulation of source/sink relations by cytokinins. Plant Growth Regul **32:** 359–367

Rolland F, Moore B, Sheen J (2002) Sugar sensing and signaling in plants. Plant Cell **14:** S185–S205

Rook F, Corke F, Card R, Munz G, Smith C, Bevan MW (2001) Impaired sucrose-induction mutants reveal the modulation of sugar-induced starch biosynthetic gene expression by abscisic acid signaling. Plant J **26:** 421–433

Sander A, Krausgrill S, Greiner S, Weil M, Rausch T (1996) Sucrose protects cell wall invertase but not vacuolar invertase against proteinaceous inhibitors. FEBS Lett **385:** 171–175

Schurr U, Schuberth B, Aloni R, Pradel KS, Schmundt D, Jähne B, Ullrich CI (1996) Structural and functional evidence for xylem-mediated water transport and high transpiration in *Agrobacterium tumefaciens*-induced tumors of *Ricinus communis*. Bot Acta **109:** 405–411

Schwalm K, Aloni R, Langhans M, Heller W, Stich S, Ullrich CI (2003) Flavonoid-related regulation of auxin accumulation in *Agrobacterium tumefaciens*-induced plant tumors. Planta DOI 10.1007/500425-003-1104-6

Sharp RE, Hsiao TC, Silk WK (1990) Growth of the maize primary root at low water potentials: II. Role of growth and deposition of hexose and potassium in osmotic adjustment. Plant Physiol **93:** 1337–1346

Smeekens S (2000) Sugar-induced signal transduction. Annu Rev Plant Physiol Plant Mol Biol **51:** 49–81

Sturm A, Sebkova V, Lorenz V, Hardegger M, Lienhard S, Unger C (1995) Development- and organ-specific expression of the genes for sucrose synthase and three isoenzymes of acid β-fructosidase in carrot. Planta **195:** 601–610

Sturm A, Tang GQ (1999) The sucrose-cleaving enzymes of plants are crucial for development, growth and carbon partitioning. Trends Plant Sci **4:** 401–407

Taylor GE, Gunderson CA (1988) Physiological site of ethylene effects on carbon dioxide assimilation in *Glycine max*. L. Merr. Plant Physiol **86:** 85–92

Troll W, Lindsley J (1955) A photometric method for the determination of proline. J Biol Chem **215:** 655–660

Tymowska-Lalanne Z, Kreis M (1998) The plant invertases: physiology, biochemistry and molecular biology. Adv Bot Res **28:** 72–117

Ullrich CI, Aloni R (2000) Vascularization is a general requirement for growth of plant and animal tumours. J Exp Bot **51:** 1951–1960

van Bel AJE (2003) The phloem, a miracle of ingenuity. Plant Cell Environ **26:** 125–149

Veselov D, Langhans M, Hartung W, Aloni R, Feussner I, Götz C, Veselova S, Schlomski S, Dickler C, Bächmann K et al. (2003) Development of *Agrobacterium tumefaciens* C58-induced plant tumors and impact on host shoots are controlled by a cascade of jasmonic acid, auxin, cytokinin, ethylene, and abscisic acid. Planta **216:** 512–522

Wächter R, Fischer K, Gäbler R, Kühnemann F, Urban W, Bögemann GM, Voeseneck LACJ, Blom CWPM, Ullrich CI (1999) Ethylene production and ACC-accumulation in *Agrobacterium tumefaciens*-induced plant tumours and their impact on tumour and host stem structure and function. Plant Cell Environ **22:** 1263–1273

Weil M, Rausch T (1990) Cell wall invertase in tobacco crown gall cells. Plant Physiol **94:** 1575–1581

Weiler EW (1982) An enzyme-immunoassay for cis-(+)-abscisic acid. Physiol Plant **54:** 510–514

Weiler EW, Schröder J (1987) Hormone genes and crown gall disease. Trends Biochem Sci **12:** 271–275

Wobus U, Weber H (1999) Sugars as signal molecules in plant seed development. Biol Chem **380:** 937–944

Xu J, Avigne WT, McCarty DR, Koch KE (1996) A similar dichotomy of sugar modulation and developmental expression affects both paths of sucrose metabolism: evidence from maize invertase gene family. Plant Cell **8:** 1209–1220

Yang NS, Russell D (1990) Maize sucrose synthase-1 promoter directs phloem-cell specific expression of *Gus* gene in transgenic tobacco plants. Proc Natl Acad Sci USA **87:** 4144–4148

Zambryski P, Tempé J, Schell J (1989) Transfer and function of T-DNA genes from *Agrobacterium* Ti and Ri plasmids in plants. Cell **56:** 193–201